Unipolar Amplifier Enabling Measurement of Far-field Intra-cardiac Electromyogram for Blood Pump Control

Seraina Anne Dual[1,2,3][a], Dominic Jacob[1], Mirko Meboldt[1][b] and Marianne Schmid Daners[2][c]

[1]*Product Development Group Zurich pd|z, ETH Zurich, Tannenstrasse 3, Zürich, Switzerland*
[2]*Radiology, Stanford University, 780 Welch Rd., Palo Alto, U.S.A.*
[3]*Cardiovascular Institute, Stanford University, 780 Welch Rd., Palo Alto, U.S.A.*

Keywords: Electromyogram, Electrophysiology, Hemodynamic Monitoring, Unipolar Amplifier, Brody Effect.

Abstract: Heart pumps are implanted as an alternative to heart transplantation in patients with heart failure. Future devices are expected to respond to the physiological need of each patient automatically. Physiological control algorithms have shown to be robust if based on the measurement of end-diastolic volume (EDV); but real-time measurements of EDV are not available. In theory, the EDV has been shown to correlate with the maximum depolarization amplitude (DA) of the intra-cardiac electromyogram (iEMG). In practice, this requires the unipolar measurement of an electric signal, which has not been attempted inside the heart. We herein present a custom-built unipolar amplifier, which we connected to a heart pump cannula prototype with four integrated off-the-shelf pacemaker electrodes. The recorded signals from the unipolar amplifier showed excellent agreement with the gold standard measurement of surface electrocardiogram (ECG) using a commercial ECG simulator and in-vivo data acquired in four pigs. We present recordings of unipolar iEMG from the cannula of a heart pump. The new unipolar amplifier makes it possible to measure the DA of the iEMG and therefore potentially provides a real-time EDV signal to heart pumps for physiological control in the future.

1 INTRODUCTION

Heart pumps are implanted in patients with heart failure as an alternative to heart transplantation (Kirklin et al., 2018). The heart pump is implanted in parallel to the heart and provides additional blood flow to supplement organ perfusion, where the level of support is determined by the pump speed. Inadequate pump speed settings can lead to serious complications such as pulmonary congestion in the case of under-pumping or suction of the myocardium in case of over-pumping (Schima et al., 2008). Physiological control algorithms based on the end-diastolic volume (EDV) of the left ventricle (LV) have proven save and robust in the experimental setting (Petrou et al., 2018; Ochsner et al., 2014; Ochsner et al., 2017). However, their implementation is hindered by the lack of real-time measurements of the EDV. A measurement of EDV could further inform the clinical management of patients with heart failure, as EDV is understood to be a surrogate of fluid status. Even if no physio-

logical control algorithm was implemented, real-time measurement of EDV could help clinicians set an appropriate pump speed or administer diuretics. However, real-time EDV measurements is unavailable to date.

The LV EDV has been suggested to correlate with the maximum electric depolarization amplitude (DA) of the heart by Brody et al in 1956 (Brody, 1956). The maximum electric signal (R-wave) coincides with the end-diastolic time point. The so-called *Brody effect* attenuates or increases a measured electric potential due conduction inhomogeneity. The blood in the LV has a higher conductivity then its surrounding and thus constitutes an inhomogeneity. The electric potential in a homogenous thorax Φ_{hom} is different from the electric potential if including the inhomogeneity of the LV blood pool Φ_{inhom} (Brody, 1956). The Brody factor is calculated as the ratio between these two electric potentials (β) (Eq. 1) and depends on the size of the LV blood pool.

$$\beta = \frac{\Phi_{inhom}}{\Phi_{hom}} \qquad (1)$$

Hence, depending on the LV EDV, the measured electric potential is increased or decreased by the Brody

[a] https://orcid.org/0000-0001-6867-8270
[b] https://orcid.org/0000-0001-5828-5406
[c] https://orcid.org/0000-0002-6411-8871

factor. Changes in the DA will correlate with changes in the EDV.

Previous studies have investigated the Brody effect in the surface electrocardiogram (ECG) (Madias et al., 2005; Amoore, 1985). The gold standard measurement of ECG is performed by obtaining the electric potential difference between two points on the body surface (DI, DII, DIII) according to the equations:

$$DI = \phi_{LA} - \phi_{RA} \qquad (2)$$

$$DII = \phi_{LL} - \phi_{RA} \qquad (3)$$

$$DIII = \phi_{LA} - \phi_{LL} \qquad (4)$$

It was shown that with respect to surface potentials, the position of the heart in the thorax is likely to affect the ECG to a much greater degree than the *Brody effect* (Amoore, 1985). The electric depolarization can also be measured using the intra-cardiac electromyogram (iEMG) inside the blood pool. Battler et al. 1980 showed that if measured in close proximity to the heart the relationship between DA and EDV inverts from positive to negative, if measured endo- or epicardially in conscious dogs (Battler et al., 1980). Furthermore, the EDV and the DA were also correlated when the iEMG was measured in the blood pool using a pig tale catheter (Dual et al., 2016). Theoretical analyses further concluded that the *Brody effect* depends strongly on the choice of reference and can only be measured with unipolar electrodes (van Oosterom, 2010), which has not been attempted so far.

We herein present a novel unipolar amplifier to assist in measuring the iEMG from electrodes deployed on the cannula of a heart pump. First, the amplifier is tested against the gold standard surface ECG measurement. Subsequently, we show unipolar measurements of iEMG in the LV blood pool in four animals.

2 METHODS

2.1 Design of Cannula and Electrodes

A dummy cannula featuring four electrodes was designed in order to facilitate positioning in the blood pool using the typical implantation procedure for heart pumps (see Figure 1). The cannula was 3D-printed from polyamid 12 (PA 12) using a selective laser sinter process. The geometry of the cannula matched the HVAD (Medtronic, Minneapolis, MN, USA) suture ring with an outer diameter of 20.6 mm. The cannula was retrofitted with two commercially available pacemaker leads (25539254 IS-1 BI, Biotronik, Germany) with two electrodes per

lead (B1-B4). The leads were attached and the cavities sealed using silicone glue (Dow Corning 732). Electrodes B3 and B4 were shielded from interaction with the myocardium, while B1 and B2 were not. The leads were connected to the data acquisition unit (DAQ) using shielded cables.

2.2 In-vivo Trial

The cannula prototype was implanted and tested in acute pig models (n = 4, female, Swiss large white).The animal housing and all procedures and protocols were approved by the Cantonal Veterinary Office (Zurich, Switzerland) under the license number 219/2016. Animal housing and all experimental procedures were in accordance with Swiss animal welfare protection law, and conform to European Directive 2010/63/EU of the European Parliament and the Council on the Protection of Animals used for Scientific Purposes, and to the Guide for the Care and Use of Laboratory Animals.

After loss of postural reflexes following premedication with ketamine (15 mg/kg), midazolam (0.5 mg/kg) and atropine (0.1-0.2 mg/kg) anesthesia was deepened by an intravenous bolus injection of propofol (1-2 mg/kg body weight) and the animals were intubated. General anesthesia was maintained with propofol (2-5 mg/kg/h, i.v.) in combination with isoflurane (1%-2.5%) by positive pressure ventilation in an air-oxygen mixture (1:1, 4-6 L/min)with an inspired oxygen fraction (FiO2) of 0.5, tidal volume of 6-8 mL/kg, a frequency of 10-15 breaths per minute and a positive end expiratory pressure (PEEP) of 5 cmH$_2$O. For intra-operative analgesia, buprenorphine (0.01 mg/kg body weight) was administered intravenously approximately 30 minutes before the cut-down and was continued throughout anesthesia. During surgery, animals received a continuous intravenous infusion of crystalloids (5-7 mL/kg/h).

For maximum control of hemodynamics, a modified cardiopulmonary bypass (CPB) was installed without oxygenator, via a single femoral vein access realized by inserting a venous CPB-cannula in the animal's femoral vein. The surface electrodes on the left arm (LA) and leg (LL) as well as on the right arm (RA) were attached using sub-dermal steel needle-electrodes.

After hemi-sternotomy was performed for access, the cannula prototype was implanted into the LV at the apex, using an HVAD suture ring, and thus mimicking a heart pump implant (see Figure 1). After completion of both surgical steps, the thoracic spreader was removed, and the suprasternal tissue closed using sutures, while the pericardium was left
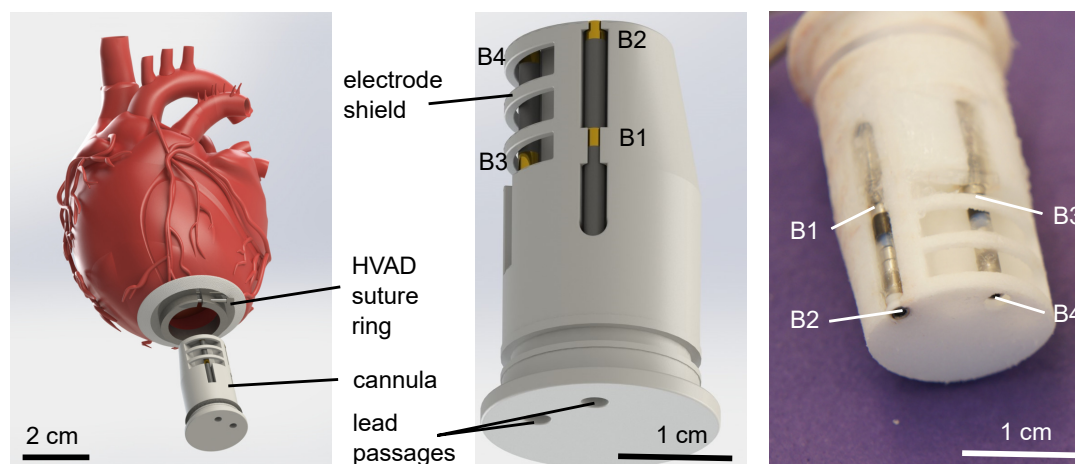
Figure 1: Cannula featuring four electrodes from pacemaker leads.

open. The thorax was re-opened only if necessary, to stabilize or resuscitate the animal.

2.3 Unipolar Amplifier

The design of the unipolar amplifier is based on the approach by Garguilo et al. (Gargiulo et al., 2013; Gargiulo, 2015). The amplifier was modified to use only one single common pseudo-infinite reference for all other channels (see Figure 2). This means, that also the reference electrode is referenced to itself and allows for signal recording. The signal is further amplified across two amplifier stages.

The goal of the reference signal was to create a pseudo-infinite potential by low-pass filtering the signal from the reference electrode. The reference electrode is filtered using a 2nd-order Sallen-Key low pass filter with a cutoff frequency of 0.034 Hz (47 μF(10%) capacitors and 100 $k\Omega$ (1%) resistors). The resulting high input impedance minimizes crosstalk with the surface ECG. Both amplifier stages are grounded through the DAQ, which is also wired to the right leg surface electrode of the animal.

The first amplifier stage consists of an INA116 instrumentation amplifier with a fixed gain, optimized to provide sufficient common-mode rejection ratio, while avoiding saturation due to DC offset voltages. The inverting input is wired to the buffered output of the pseudo-infinite reference. The measuring electrode connects to a 100 $k\Omega$ coupling resistor and then buffered and forwarded to the non-inverting input of the INA116. The guard terminal of the non-inverting input is connected to the shield of the measuring electrode. Of note, the first differential amplifier stage does not remove high frequency, as the two input signals are not identical in their noise levels. High frequency noise is reduced by band pass filter.

Between the two amplifier stages we implemented a high pass followed by a low pass filter. The high pass attenuates offsets and low frequency drift to increase to achievable gain in the second amplifier stage. The high pass was implemented as a first order active high pass with a cutoff frequency of 0.015 Hz (47 μF(10%) capacitors and 220 $k\Omega$(1%) resistors). The low pass was implemented as a 2nd-order Sallen-Key filter 590 Hz to suppress high frequency noise and attenuate signals close to and above the Nyquist Frequency (1 kHz)(27 $k\Omega$(1%) resistors and 10 nF(5%) capacitors).

The second amplifier stage (INA128) features an adjustable gain to adapt to variable electrode impedances and the unknown value of the iEMG amplitude. The inverting input of the second amplifier stage is wired to ground. The reference terminal is connected to the inverting input of the signal conditioner, allowing the amplifier to supply signals to DAQs floating at different levels. If the signal conditioner is a differential type, the inverting DAQ input is connected to the DAQ ground by the jumper to provide a reference level. If the signal conditioner is a single ended type, the jumper is left open, as the single ended inverting input provides a ground reference itself.

The design illustrated in Figure 2 can be scaled to any number of channels by replicating the circuitry in the grey box for each channel. The rest of the circuit is needed once, independent of the number of channels.

2.4 Data Acquisition

All data was acquired using the ACQ 7700 (Data Science International, St. Paul, MN, USA). A Windows machine running the Ponemah software logged the data at a sampling frequency of 2000 Hz. The in-
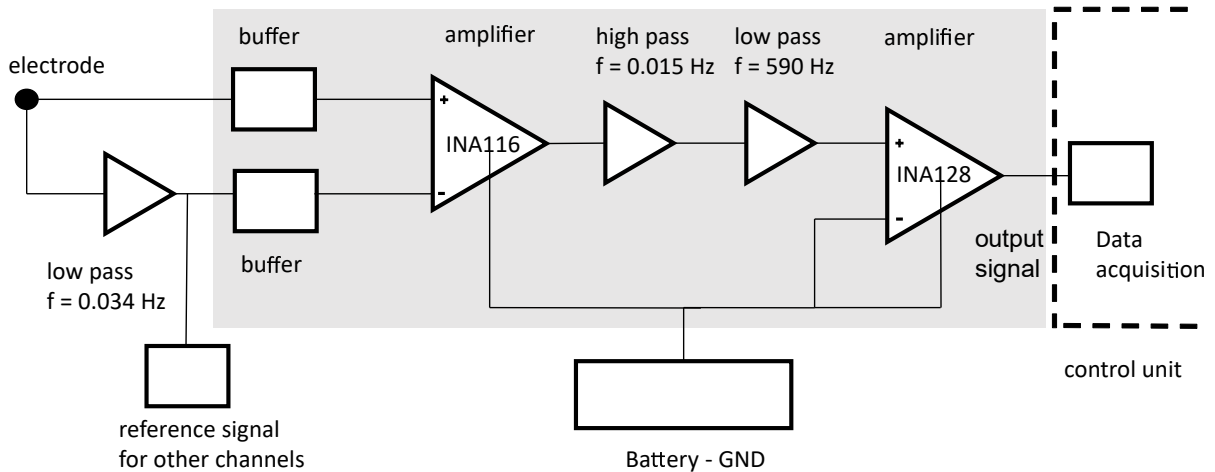
Figure 2: Schematic of the unipolar amplifier circuit.

put range of the Universal XE Signal Conditioner and the Advanced Basic DC4 Signal Conditioners were set to ±5 V. The Universal XE operated as a differential signal conditioner and the Advanced Basic DC4 operated in single ended mode. The unipolar amplifier was connected to the Advanced Basic DC4 Signal conditioner. As Gold Standard surface ECG we used a Multi-Lead Pod connected to the digital Communication Module.

2.5 Experimental Protocol

The unipolar amplifier was tested against the gold standard using (1) an ECG generator (Prosim 8, Fluke Biomedical, Washington, USA) and (2) in-vivo measurements of surface ECG in four pigs.

The Gold standard records the differentials between leads denoted as DI, DII and DIII. The unipolar amplifier measures single potentials denoted as left arm (ϕ_{LA}), left leg (ϕ_{LL}) and right leg (ϕ_{RL}). The differential leads (DI, DII, DIII) were reconstructed from the unipolar ECGs for comparison according to equations 2,3 and 4.
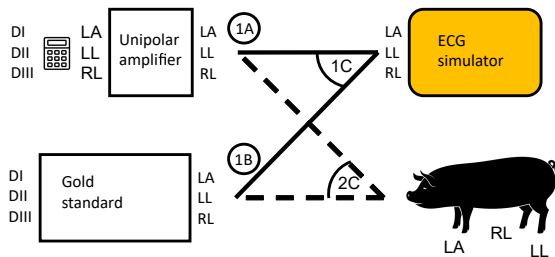

Figure 3: Schematic of the experimental setup.

The first step consisted of three configurations (see Figure 3): (1A) Unipolar amplifier - ECG simulator; (1B) Gold standard - ECG simulator; (1C) Unipo-

lar amplifier and Gold standard - ECG simulator. In the second step, the Unipolar amplifier and the Gold standard ECG amplifier were connected to the surface electrodes on the LA, LL and RA of each of the pigs (2C). In the last step, the unipolar amplifier was connected to the four electrodes on the cannula instead (see Figure 4). Each protocol was repeated four times and each measurement consisted of 15s of recorded signal length.
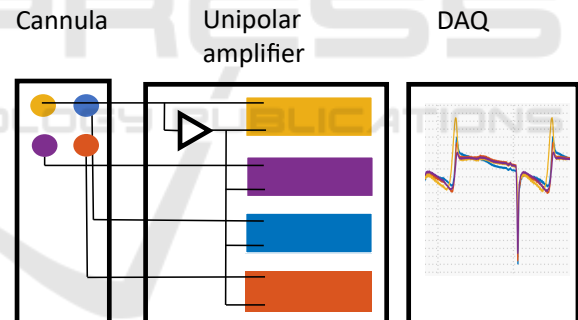

Figure 4: Connections cannula and unipolar amplifier.

2.6 Data Processing

A median filter of length three samples was used to smooth the signal. A high pass filter eliminated remaining low frequency drifts. The high pass filter was realized with a minimum order infinite impulse response filter with a passband frequency of 0.05 Hz and a stopband frequency of 0.01 Hz. Finally, a 6th order notch filter with a center frequency of 50 Hz and a -3dB bandwidth of 0.5 Hz was implemented and a low pass filter removed additional high frequency noise with a cutoff frequency of 250 Hz.

2.7 Data Analysis

2.7.1 Crosstalk

Crosstalk can occur during simultaneous measurements of surface ECG leads and the iEMG using the same amplifier. Crosstalk was assessed by comparing measurements of each amplifier alone (1A, 1B) and together (1C). Only differential measurements were compared, computed using equations 2, 3, and 4. The ECG without crosstalk is denoted as $\overline{ECG}$ and the one with possible crosstalk is denoted as $\widetilde{ECG}$. If no crosstalk is present and noise neglected, then $\overline{ECG} = \widetilde{ECG}$ holds. The normalized root mean square error (NRMSE), the DA and the ECG's signal power were used as performance indicator (●). The NRMSE is computed as follows, using the root mean square (RMS):

$$\widehat{NRMSE} = \frac{RMS(\widetilde{ECG} - \overline{ECG})}{RMS(\overline{ECG})} \quad (5)$$

Furthermore, we compute the error in detecting DA calculated as relative number according to (equation 6).

$$\widehat{NDAE} = \frac{\widetilde{DA} - \overline{DA}}{\overline{DA}} \quad (6)$$

2.7.2 Comparison Unipolar Amplifier vs. Gold Standard

The comparison between the unipolar and the gold standard amplifier was done using the simultaneously acquired data of both the ECG simulator (1C) and the in-vivo data (2C). The signal of the gold standard amplifier served as reference, while the reconstructed differential leads from the unipolar amplifier ECGs were compared to it. The same performance indicators as in the previous section were computed, with minor adjustments as displayed in equations 6 and 7.

$$\widehat{NRMSE} = \frac{RMS(ECG|_{UP} - ECG|_{GS})}{RMS(ECG|_{GS})} \quad (7)$$

$$\widehat{DA} = \frac{DA|_{UP}}{DA|_{GS}} \quad (8)$$

3 RESULTS

3.1 Crosstalk Quantification

The crosstalk between the unipolar amplifier and the gold standard amplifier were tested on the ECG simulator. The values of the performance indicators are shown in Table 1 for the gold standard amplifier and in Table 2 for the unipolar amplifier. The $\widehat{NRMSE}$ remained below 2% in all three surface leads. The error of the estimated DA also remained below 2%. The sum of the power from 0.05 Hz to 250 Hz remained constant over the crosstalk test with an error of less than 5%. We conclude that our amplifier measures the surface and intra-cardiac potentials independently from each other. A simultaneous measurement is advantageous, because we can then report the effect of changes in LV volume for both the surface ECG as well as the intra-cardiac iEMG. The surface ECG may be confounded by a change in distance between the heart and the chest wall. The unipolar iEMG, however, should allow for measurement of the Brody effect.

Table 1: Crosstalk of gold standard.

	Gold Standard	
	$\widehat{NRMSE}$	$\widehat{NDAE}$
Unit	[%]	[%]
A1-DI	0,37	-0,10
A1-DII	0,67	0,00
A1-DIII	0,52	0,00
A2-DI	0,45	0,15
A2-DII	0,34	0,31
A2-DIII	0,30	-0,10
A3-DI	0,34	0,61
A3-DII	0,41	0,58
A3-DIII	0,45	-0,50
A4-DI	0,43	-0,34
A4-DII	0,31	-0,66
A4-DIII	0,30	0,50

Table 2: Crosstalk of unipolar amplifier.

	Unipolar Amplifier	
	$\widehat{NRMSE}$	$\widehat{NDAE}$
Unit	[%]	[%]
A1-DI	0,37	0,00
A1-DII	0,34	-0,17
A1-DIII	0,32	1,09
A2-DI	0,72	-0,31
A2-DII	1,54	-1,01
A2-DIII	1,21	0,00
A3-DI	0,39	-0,24
A3-DII	0,34	0,51
A3-DIII	0,33	-1,43
A4-DI	0,35	0,00
A4-DII	0,34	0,00
A4-DIII	0,32	-0,41

3.2 Performance of 50 Hz Notch Filter

The 50 Hz notch filter was assessed using a single surface electrode (ϕ_{RA}) measured against the pseudo-infinite potential (Figure 5). In the top panel, the amplifier was wired to the ECG simulator (1C) and in the bottom panel to the animal (2C). The signal was filtered with a 6th order notch filter at 50 Hz. The root mean square error was calculated under the assumption that the filtered signal was the true signal. The resulting RMSE for the signal obtained from the ECG simulator is 0.04 mV. The error for the in-vivo data was 0.24 mV, and increased with respect to the value obtained in the ECG simulator. The 50 Hz notch filter was critical in obtaining an undisturbed signal. The large amount of digital equipment in the laboratory facilities introduced a high amount of noise. We expect this to be true to a similar extent if such a device was implemented in the clinical context.
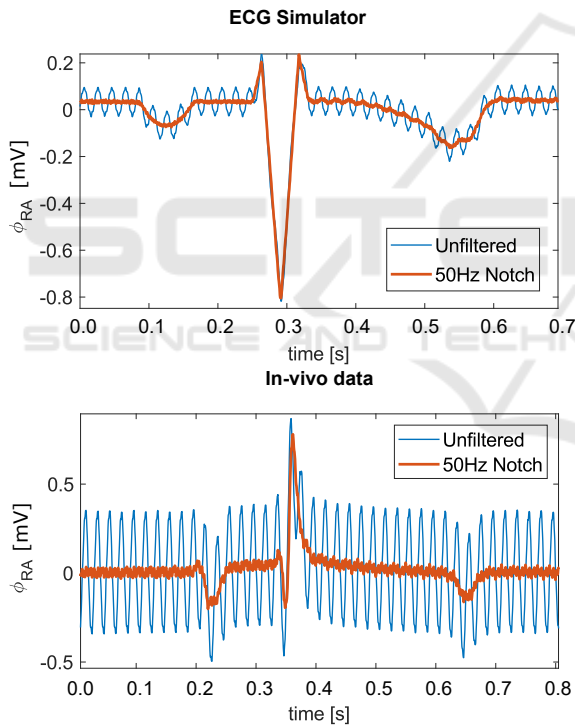

Figure 5: Reduction of 50 Hz noise using notch filter.

3.3 Comparison of Unipolar Amplifier vs. Gold Standard

We compare the surface lead ECGs measured by the unipolar and the gold standard amplifier for both simulated ECGs (see Table 3) and data obtained in-vivo (see Table 4). A representative example of a time series data is shown in Figure 6. While connected to the ECG simulator, the respective errors are within the

range of what was observed during the crosstalk experiments (Section 3.1). The $\widehat{NRMSE}$ was below 1% during all tests. The values of the performance indicators $\widehat{DA}$ remained below 1.5%. The unipolar amplifier measured the same potentials as the gold standard, despite relying on a pseudo-infinite potential as a reference.

Table 3: ECG Simulator Unipolar Amplifier vs. Gold Standard.

| | ECGSimulator | |
	$\widehat{NRMSE}$	$\widehat{NDAE}$
Unit:	[%]	[%]
A1-DI	0,39	0,50
A1-DII	0,52	0,90
A1-DIII	0,43	-0,67
A2-DI	0,40	0,70
A2-DII	0,83	0,12
A2-DIII	0,72	1,44
A3-DI	0,39	0,51
A3-DII	0,35	0,18
A3-DIII	0,32	1,03
A4-DI	0,35	0,70
A4-DII	0,32	0,63
A4-DIII	0,29	0,71

In-vivo, the errors increase as more environmental disturbances and noise are picked up by the amplifiers (see Figure 5). The $\widehat{NRMSE}$ of the signal remained below 5% for 10 out of 12 measurements. The deviations were especially high in Animal 2 (A2), which also showed a variable heart rhythm. Deviations in the detection of the DA ($\widehat{DA}$) were found to be less than 5% in 9 out of 10 evaluated ECGs. The very high value for A3-DII originated from an error in the signal processing of the maximum DA peak detection. The errors in differential lead DII were mostly higher, when compared to the DI and DIII lead. It is important to note that we report relative error values, such that the low signal strength of DII results in unfavorable error values.

An ideal amplifier has minimal low frequency drift. In Figure 5 on the right we can see a deviation of the red signal from the iso-electric line. The signal measured by the gold standard amplifier is confounded by a low frequency drift. In this particular example, the unipolar amplifier outperformed the gold standard measurement. Any reported error values might thus be confounded by low frequency drift in the gold standard amplifier.

In summary, the accuracy of measuring unipolar surface leads is accurate enough and the concept of using a unipolar measurement works.
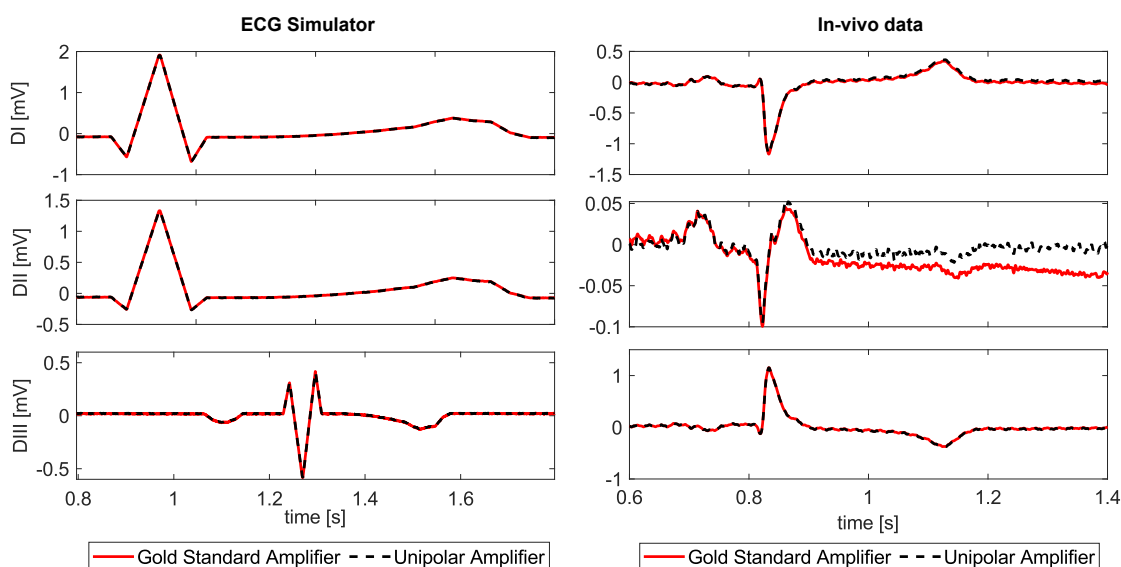
Figure 6: Comparison between Gold Standard and Unipolar Amplifier.

Table 4: In-Vivo Unipolar Amplifier vs. Gold Standard.

	In-vivo	
	$\widehat{NRMSE}$	$\widehat{NDAE}$
Unit:	[%]	[%]
A1-DI	-	-
A1-DII	0,83	-1,18
A1-DIII	-	-
A2-DI	5,17	3,46
A2-DII	2,10	2,75
A2-DIII	6,17	1,15
A3-DI	1,81	-0,50
A3-DII	2,59	-92,57
A3-DIII	2,62	2,83
A4-DI	1,31	0,01
A4-DII	1,91	1,93
A4-DIII	0,85	-0,73

3.4 Effect of Post-processing of Depolarization Amplitude

The effect of post-process filtering is displayed in Figure 7. We estimated the amount of 50 Hz noise, by applying an additional 50 Hz filter and calculating the error between the filtered and the original signal. The ECG lead II was used for this analysis. In the surface ECG, a 50 Hz noise with amplitude of 0.018 mV was present with a DA of 0.61 mV (3%). In the iEMG leads, the 50Hz noise amplitude equals approximately 5% (0.63 mV) of the DA. The noise reduction and the distortion of the ECG signal and DA due to the filters is shown in Figure 7. Post-processing of the acquired signals using an additional 50 Notch filter and a lowpass filter was found to be necessary and feasible

without losing any signal amplitude of the DA.

3.5 Intra-cardiac Electromyogram

All four intra-cardiac electromyograms could be acquired synchronously with one intra-cardiac electrode chosen as reference. An example of the far-field intra-cardiac signals obtained in Animal 2 is shown in Figure 8. The surface ECG shows a normal rhythm in all three leads DI, DII, and DIII. The recordings between the four unipolar intra-cardiac electrodes are highly similar. However, the shape of the iEMG waveform (B1-B4) is distinctly different compared to the surface leads (DI-DIII). The R-wave in the surface ECG coincides with the intra-cardiac depolarization amplitude. Still, the intra-cardiac potentials show another distinct peak originating from the re-polarization at the end of the cardiac cycle. The re-polarization is less distinct in the surface recordings.

3.6 Implications for Blood Pump Control

The proposed technology constitutes and important step towards integrated real-time measurement of EDV for blood pump control. The real-time measurement of LV volume has been attempted previously using alternative measurement principles. Four ring-shaped electrodes were integrated into the cannula of a heart pump to allow for a measurement of electric impedance (Cysyk et al., 2018). The outer two electrodes span an electric field, while the inner electrodes record changes in resistance. The technology showed limited sensitivity, mainly because the measurement
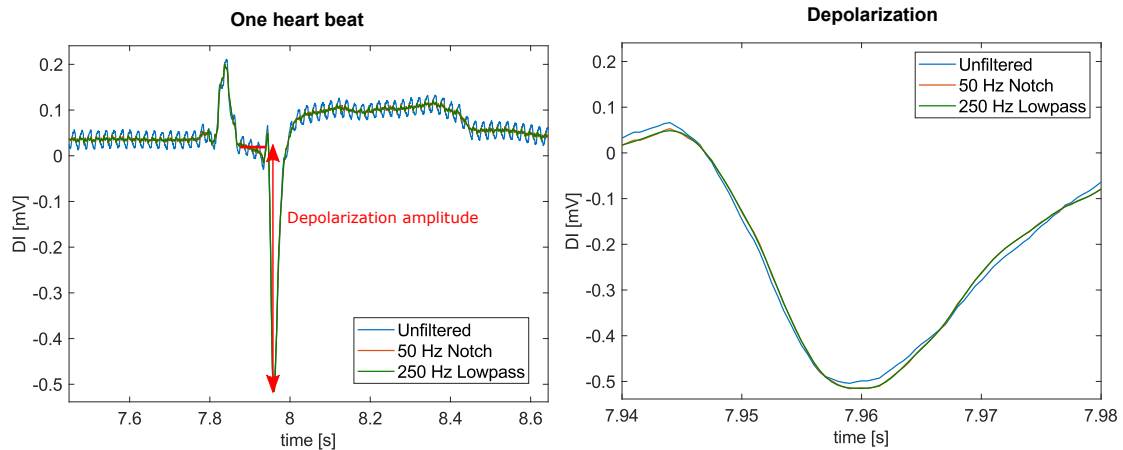
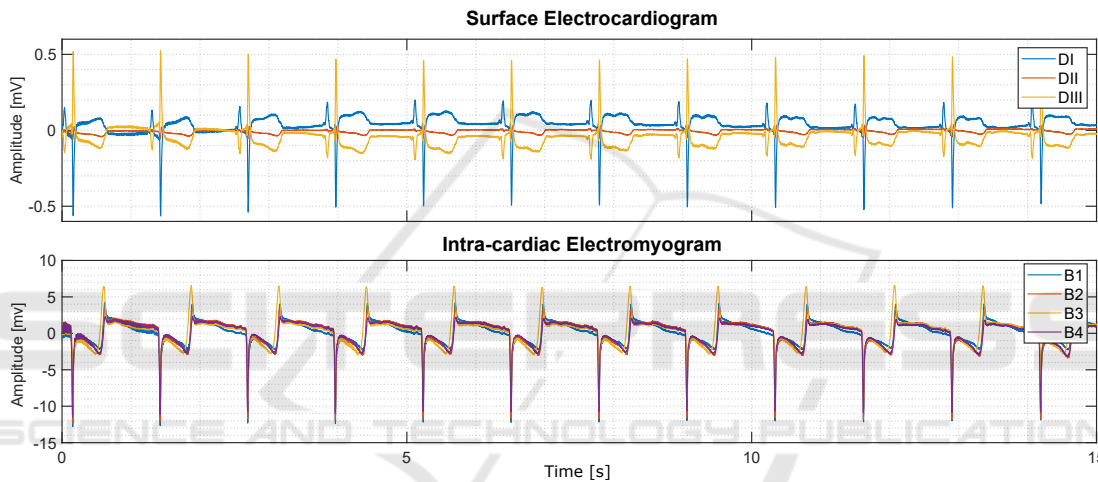Figure 7: Effect of filtering on the measurement of the depolarization amplitude.

Figure 8: Surface (top) and intra-cardiac electromyogram (bottom).

was limited to the blood pool immediately surrounding the cannula. The motivation for developing this unipolar amplifier was to allow for a far-field electric measurement of the entire LV blood pool. Another promising approach makes use of electric impedance measurement across implantable defibrillator leads (Haines et al., 2017). As most patients with heart failure have a pacemaker, this could be feasible but would require communication across devices. Alternatively, ultrasonic concepts have been proposed and studied but their applicability remains limited considering the complexity of integrating such technology in an implantable device (Dual et al., 2019).

Blood pump control requires an accuracy in EDV of 20% for robust control. As a next step, the unipolar amplifier will be used to study how accurate we can estimate the EDV from the proposed unipolar iEMG measurements. Furthermore, the influence of the hematocrit needs to be carefully assessed. Provided positive results, the iEMG could enable blood

pump control based on the EDV using established electrode technology.

4 CONCLUSIONS

We herein present a method to measure the unipolar intra-cardiac electro-myogram using a novel amplifier. The design enables accurate detection of the depolarization amplitude in the intra-cardiac blood pool and will allow us to investigate the relationship between iEMG and the EDV (Brody-effect) in the future. The unipolar amplifier reproduces the gold standard differential ECG measurements with minimal errors. The unipolar amplifier is thus capable of measuring electric potentials in a robust and accurate way. Furthermore, the post-processing methodology enables the preservation of the peak depolarisation amplitude, despite significant noise. This technical work will enable future investigations of the Brody

effect during changes in left ventricular volume. The current design is limited by the use of the right leg of the animal as ground for the data acquisition software. Furthermore, the current design of the unipolar amplifier does not actively isolate the subject from the DAQ. The performance of a fully portable system will need to be re-evaluated using a similar experimental setup as proposed in this paper.

ACKNOWLEDGEMENTS

REFERENCES

Amoore, J. N. (1985). The brody effect and change of volume of the heart. *Journal of Electrocardiology*, 18(1):71–75.

Battler, A., Froelicher, V. F., Gallagher, K. P., Kumada, T., McKown, D., Kemper, W. S., and Ross, J. (1980). Effects of changes in ventricular size on regional and surface QRS amplitudes in the conscious dog. *Circulation*, 62(1):174–180.

Brody, D. A. (1956). A Theoretical Analysis of Intracavitary Blood Mass Influence on the Heart-Lead Relationship. *Circulation Research*, IV:731–737.

Cysyk, J., Newswanger, R., Popjes, E., Pae, W., Jhun, C.-S., Izer, J., Weiss, W., and Rosenberg, G. (2018). Cannula Tip With Integrated Volume Sensor for Rotary Blood Pump Control: Early-Stage Development. *ASAIO journal*.

Dual, S. A., Ochsner, G., Petrou, A., Amacher, R., Wilhelm, M., Meboldt, M., and Schmid Daners, M. (2016). R-Wave Magnitude : a Control Input for Ventricular Assist Devices. *International Workshop on Biosignal Interpretation, Osaka*.

Dual, S. A., Zimmermann, J. M., Neuenschwander, J., Cohrs, N. H., Solowjowa, N., Stark, W. J., Meboldt, M., and Schmid Daners, M. (2019). Ultrasonic sensor concept to fit a ventricular assist device cannula evaluated using geometrically accurate heart phantoms. *Artificial Organs*, 43(5):467–477.

Gargiulo, G. D. (2015). True Unipolar ECG Machine for Wilson Central Terminal Measurements. *BioMed Research International*, 2015.

Gargiulo, G. D., McEwan, A. L., Bifulco, P., Cesarelli, M., Jin, C., Tapson, J., Thiagalingam, A., and Van Schaik, A. (2013). Towards true unipolar bio-potential recording: A preliminary result for ECG. *Physiological Measurement*, 34(1).

Haines, D. E., Wong, W., Canby, R., Jewell, C., Houmsse, M., Pederson, D., Sugeng, L., Porterfield, J., Kottam, A., Pearce, J., Valvano, J., Michalek, J., Trevino, A., Sagar, S., and Feldman, M. D. (2017). Validation of a defibrillation lead ventricular volume measurement compared to three-dimensional echocardiography. *Heart Rhythm*, 14(10):1515–1522.

Kirklin, J. K., Xie, R., Cowger, J., de By, T. M., Nakatani, T., Schueler, S., Taylor, R., Lannon, J., Mohacsi, P., Gummert, J., Goldstein, D., Caliskan, K., and Hannan, M. M. (2018). Second annual report from the ISHLT Mechanically Assisted Circulatory Support Registry. *The Journal of Heart and Lung Transplantation*, 37(6):685–691.

Madias, J. E., Song, J., White, C. M., Kalus, J. S., and Kluger, J. (2005). Response of the ECG to Short-Term Diuresis in Patients with Heart Failure. *Annals of Noninvasive Electrocardiology*, 10(3):288–296.

Ochsner, G., Amacher, R., Wilhelm, M. J., Vandenberghe, S., Tevaearai, H., Plass, A., Amstutz, A., Falk, V., and Schmid Daners, M. (2014). A Physiological Controller for Turbodynamic Ventricular Assist Devices Based on a Measurement of the Left Ventricular Volume. *Artificial organs*, 38(7):527–538.

Ochsner, G., Wilhelm, M. J., Amacher, R., Petrou, A., Cesarovic, N., Staufert, S., Röhrnbauer, B., Maisano, F., Hierold, C., Meboldt, M., and Schmid Daners, M. (2017). In Vivo Evaluation of Physiologic Control Algorithms for Left Ventricular Assist Devices Based on Left Ventricular Volume or Pressure. *ASAIO Journal*, 63(5):568–577.

Petrou, A., Lee, J., Dual, S., Ochsner, G., Meboldt, M., and Schmid Daners, M. (2018). Standardized Comparison of Selected Physiological Controllers for Rotary Blood Pumps: In Vitro Study. *Artificial Organs*, 42(3):E29–E42.

Schima, H., Trubel, W., Moritz, A., Wieselthaler, G., Stohr, H. G., Thoma, H., Losert, U., and Wolner, E. (2008). Noninvasive Monitoring of Rotary Blood Pumps: Necessity, Possibilities, and Limitations. *Artificial Organs*, 16(2):195–202.

van Oosterom, A. (2010). Macroscopic Source Descriptions. In Macfarlane, P., van Oosterom, A., Pahlm, O., Kligfield, P., Janse, M., and Camm, J., editors, *Comprehensive Electrocardiology*, pages 193–225. Springer Verlag, London, 2011 edition.